appreciable separation between T_g and T_x. Therefore, even partial densification requires very high pressures (more than 500 MPa)[25,26] to activate dislocation-controlled, crystalline plasticity. In contrast, we have found that suitable kinetic windows do exist in the CaO–Al_2O_3, La_2O_3–TiO_2 and BaO–TiO_2 systems, which allowed us to perform bulk consolidation of rapidly quenched glass beads in a similar fashion to that for Al_2O_3–REO. On the basis of these results we believe that, as for bulk metallic glasses, the present glass-forming and consolidation approach is applicable to a large variety of ionic compositions and will open the door to many new bulk oxide glasses and nanocrystalline ceramics. □

Received 12 March; accepted 3 June 2004; doi:10.1038/nature02729.

1. Sun, K.-H. Aluminate glasses. *Glass Ind.* **30,** 199–200, 232 (1949).
2. Sarjeant, P. T. & Roy, R. in *Reactivity of Solids* (eds Mitchell, J. W., DeVries, R. C., Roberts, R. W. & Cannon, P.) 725–733 (Wiley, New York, 1969).
3. Weber, J. K. R., Abadie, J. G., Hixson, A. D., Nordine, P. & Jerman, G. A. Glass formation and polyamorphism in rare-earth oxide-aluminum oxide compositions. *J. Am. Ceram. Soc* **83,** 868–872 (2000).
4. Weber, R., Nordine, P. C., Key, T. & Tangeman, J. in *Proceedings of the SPIE – The International Society for Optical Engineering* Vol. 4990 (eds Shibin, J. & Jacques, L.) 70–76 (SPIE – Int. Soc. Opt. Eng., Bellingham, WA, 2003).
5. Liao, S.-C., Chen, Y.-J., Kear, B. H. & Mayo, W. E. High pressure/low temperature sintering of nanocrystalline alumina. *Nanostruct. Mater.* **10,** 1063–1079 (1998).
6. Chen, I.-W. & Wang, X.-H. Sintering dense nanocrystalline ceramics without final-stage grain growth. *Nature* **404,** 168–171 (2000).
7. Klement, W., Willens, R. & Duwez, P. Non-crystalline structure in solidified gold-silicon alloys. *Nature* **187,** 869–870 (1960).
8. Turnbull, D. & Cohen, M. H. Composition requirements for glass formation in metallic and ionic systems. *Nature* **189,** 131–132 (1961).
9. Rawson, H. *Inorganic Glass-forming Systems* 23–29 (Academic, New York, 1967).
10. Jantzen, C. M., Krepski, R. P. & Herman, H. Ultra-rapid quenching of laser-melted binary and unary oxides. *Mat. Res. Bull.* **15,** 1313–1326 (1980).
11. McMillan, P. & Piriou, B. Raman spectroscopy of calcium aluminate glasses and crystals. *J. Non-Cryst. Solids* **55,** 221–242 (1983).
12. Shelby, J. E. Formation and properties of calcium aluminosilicate glasses. *J. Am. Ceram. Soc* **68,** 155–158 (1985).
13. Yajima, S., Okamura, K. & Shishido, T. Glass formation in the Ln-Al-O system (Ln: Lanthanoid and ytrrium elements). *Chem. Lett. (Jpn.)* **8,** 1313–1326 (1980).
14. Kawamura, Y., Kato, H. & Inoue, A. Full strength compacts by extrusion of glassy metal powder at the supercooled liquid state. *Appl. Phys. Lett.* **67,** 2008–2013 (1995).
15. Waku, Y., Ohtsubo, H. & Inoue, A. A jelly-like ceramic fiber at 1193 K. *Mat. Res. Innovat.* **3,** 185–189 (2000).
16. Sarjeant, P. T. & Roy, R. Ti^{4+} coordination in glasses in RO-TiO_2 systems. *J. Am. Ceram. Soc.* **52,** 57–58 (1969).
17. Inoue, A., Zhang, T. & Masumoto, T. Glass-forming ability of alloys. *J. Non-Cryst. Solids* **156–158,** 473–480 (1993).
18. Shelby, J. E. & Kohli, J. T. Rare-earth aluminosilicate glasses. *J. Am. Ceram. Soc* **73,** 39–42 (1990).
19. Angell, C. A. Structural instability and relaxation in liquid and glassy phases near the fragile liquid limit. *J. Non-Cryst. Solids* **102,** 205–221 (1988).
20. Beall, G. H. in *Advances in Nucleation and Crystallization in Glasses* (eds Hench, L. L. & Freiman, S. W.) 251–261 (American Ceramic Society, Columbus, Ohio, 1971).
21. Rosenflanz, A. *Fused Al_2O_3-Rare-Earth oxide-ZrO_2 Eutectic Materials*. US Patent 6,582,488 (2003)
22. Beall, G. H. & Pinckney, L. R. Nanophase glass-ceramics. *J. Am. Ceram. Soc* **82,** 5–16 (1999).
23. Mizuta, H. *et al.* Preparation of high-strength and translucent alumina by hot isostatic pressing. *J. Am. Ceram. Soc.* **75,** 469–473 (1992).
24. Yip, S. Nanocrystals: the strongest size. *Nature* **391,** 532–533 (1998).
25. Kear, B. H., Liao, S.-C. & Mayo, W. E. *High Pressure and Low Temperature Sintering of Nanophase Ceramic Powders.* US Patent 6,395,214 (2002).
26. Freim, J., McKittrick, J., Nellis, W. J. & Katz, J. D. Development of novel microstructures in zirconia-toughened alumina using rapid solidification and shock compaction. *J. Mater. Res.* **11,** 110–119 (1996).
27. Wilding, M. C. & McMillan, P. F. Polyamorphic transitions in yttria-alumina liquids. *J. Non-Cryst. Solids* **293–295,** 357–365 (2001).
28. Bansal, N. P. *Handbook of Glass Properties* Ch. 11 (Academic, New York, 1986).
29. McMillan, P. W. in *Glass-ceramics* (eds Roberts, J. P. & Popper, P.) 196–200 (Academic, New York, 1979).

Supplementary Information accompanies the paper on **www.nature.com/nature**.

Acknowledgements We thank C. Goodbrake (3M Company) for help with microscopy, and I.-W. Chen (University of Pennsylvania) for helpful comments during the preparation of the manuscript.

Competing interests statement The authors declare competing financial interests; details accompany the paper on **www.nature.com/nature**.

Correspondence and requests for materials should be addressed to A.R. (arosenflanz@mmm.com).

Self-assembly of amphiphilic dendritic dipeptides into helical pores

Virgil Percec[1], Andrés E. Dulcey[1], Venkatachalapathy S. K. Balagurusamy[1,2], Yoshiko Miura[1], Jan Smidrkal[1], Mihai Peterca[1,2], Sami Nummelin[1], Ulrica Edlund[1], Steven D. Hudson[3], Paul A. Heiney[2], Hu Duan[3], Sergei N. Magonov[4] & Sergei A. Vinogradov[5]

[1]*Roy & Diana Vagelos Laboratories, Department of Chemistry, University of Pennsylvania, Philadelphia, Pennsylvania 19104-6323, USA*
[2]*Department of Physics and Astronomy, University of Pennsylvania, Philadelphia, Pennsylvania 19104-6396, USA*
[3]*National Institute of Standards and Technology, Gaithersburg, Maryland 20899-8544, USA*
[4]*Digital Instruments, Veeco Metrology Group, Santa Barbara, California 93110, USA*
[5]*Department of Biochemistry and Biophysics, University of Pennsylvania, Philadelphia, Pennsylvania 19104-6059, USA*

Natural pore-forming proteins act as viral helical coats[1] and transmembrane channels[2–4], exhibit antibacterial activity[5] and are used in synthetic systems, such as for reversible encapsulation[6] or stochastic sensing[7]. These diverse functions are intimately linked to protein structure[1–4]. The close link between protein structure and protein function makes the design of synthetic mimics a formidable challenge, given that structure formation needs to be carefully controlled on all hierarchy levels, in solution and in the bulk. In fact, with few exceptions[8,9], synthetic pore structures capable of assembling into periodically ordered assemblies that are stable in solution and in the solid state[10–13] have not yet been realized. In the case of dendrimers, covalent[14] and non-covalent[15] coating and assembly of a range of different structures[15–17] has only yielded closed columns[18]. Here we describe a library of amphiphilic dendritic dipeptides that self-assemble in solution and in bulk through a complex recognition process into helical pores. We find that the molecular recognition and self-assembly process is sufficiently robust to tolerate a range of modifications to the amphiphile structure, while preliminary proton transport measurements establish that the pores are functional. We expect that this class of self-assembling dendrimers will allow the design of a variety of biologically inspired systems with functional properties arising from their porous structure.

The dendron (4-3,4-3,5)12G2-X with X = CO_2CH_3 and CO_2H, and the dendron (4-3,4-3,5)*n*G2-CH_2OH with n = 10–16, self-assemble into closed supramolecular columns[18]. The dendrons (4-3,4-3,5)12G2-CH_2-X containing as X-groups Boc(Moc)-L-Tyr-L-Ala-OMe, Boc-D-Tyr-D-Ala-OMe, Boc-L-Tyr-D-Ala-OMe, Boc-D-Tyr-L-Ala-OMe, Boc-DL-Tyr-DL-Ala-OMe and Moc-L-Tyr-L-OMe (Fig. 1a) were synthesized (Supplementary Schemes SS1 and SS2), and their dipeptide groups (short names for Boc-L-Tyr-L-Ala-OMe are L-Tyr-L-Ala or L-L dipeptide) were used as tags to monitor self-assembly and expression of chirality in solution and in bulk (Boc, *t*-butoxycarbonyl; Moc, methoxycarbonyl). In solvents allowing hydrogen-bonding, such as $CHCl_3$, CH_2Cl_2 and tetrahydrofuran (THF), self-assembly is not detected by temperature- and concentration-dependent ^{1}H-NMR, UV spectroscopy or circular dichroism (CD). This indicates that the equilibrium between the trans and gauche conformers of the benzyl ether moiety favours a globular dendron conformation encapsulating the dipeptide in its focal point (Fig. 1), thereby sterically prohibiting intermolecular hydrogen-bonding.

In contrast, hydrogen-bonding and self-assembly occur in the

©2004 Nature Publishing Group

solvophobic solvent cyclohexane: regardless of dipeptide stereochemistry, a decrease in temperature from 60 °C to 30 °C leads to a downfield shift of the NH protons of Tyr and Ala and of CH of Tyr (deshielding), and an upfield shift of the aromatic, benzyl and methylenic ether protons of the dendron, indicative of hydrogen-bonding and shielding effects due to intermolecular interactions (Fig. 2a). The chemical shifts of methyl, methoxy and CH groups of Ala are not affected. Below 30 °C, the ^{1}H-NMR spectrum broadens, corresponding to stiffening of the supramolecular structure. Except for the alkyl groups, no NMR spectrum is detected below 24 °C (Fig. 2a), indicating decreased molecular motion[19,20]. On cooling from 60 °C to 42 °C, an increase in the absorption at 230 nm (A_{230}) of the UV spectrum (hyperchromic effect) and a blue shift are observed in cyclohexane (Fig. 2b). A_{230} is constant between 42 °C and 30 °C; upon cooling from 30 °C to 12 °C, a second blue shift of the A_{230} peak (hypochromic effect) and an isosbestic point are observed. The hypochromic effect[19] is indicative of oriented chromophores, varying with their conformation and distance. Below 12 °C, the UV absorption spectrum shows no observable changes. Plotting A_{230} as a function of temperature yields a sigmoidal curve, indicative of a cooperative two-state process for self-assembly[20,21]. In addition, the increase of A_{230} from 60 °C to 42 °C is associated with the transition from a globular dendron containing a mixture of trans and gauche benzyl ether conformers to an all trans-tapered dendron that facilitates self-assembly (Fig. 1). During this process, intramolecular interactions within the globular dendron are eliminated (causing the hyperchromic effect) and the trans-tapered dendron undergoes intermolecular hydrogen-bonding (Fig. 2a, b). Below 32 °C, the hypochromic and blue shift and the appearance of the isosbestic point indicate an equilibrium between the tapered dendron and its aggregate. At about 12 °C, this equilibrium is shifted entirely to the supramolecular aggregate.

CD experiments detect chirality in the supramolecular structure, and thus complement the ^{1}H-NMR and UV analysis. Chiral dipeptides in THF and chiral dendritic dipeptides in THF, CH_2Cl_2, $CHCl_3$ and $ClCH_2CH_2Cl$ show in the CD spectra between 60 °C and 8 °C only the ellipticity of the dipeptide chromophore at $\lambda = 232$ nm, indicating molecular solutions (Supplementary Figs SF1 to SF3). Regardless of temperature and concentration, the CD of racemic (4-3,4-3,5)12G2-CH_2-(DL-Tyr-DL-Ala) does not exhibit any signal in cyclohexane or in other solvents (Supplementary Fig. SF2). From 60 °C to 30 °C, both the L-L and D-D dendritic dipeptides exhibit in cyclohexane only the ellipticity of the dipeptide (Fig. 2c, d and Supplementary Fig. SF3). These results, together with UV and NMR data (Fig. 2a, b), indicate that the dendron adopts an all-trans tapered conformation and is in fast exchange with its aggregate. Below 30 °C, only the trans-tapered conformer exists in molecular solution. In this temperature range, the transfer of chirality from the dipeptide to the aromatic part of the dendron, amplification of the Cotton effects and an isodichroic point are observed. This implies that the supramolecular aggregate must have an architecture equipped with a mechanism capable of amplifying the stereochemical information of the dipeptide. The plots of the chemical shifts (Fig. 2a) and ellipticity [Θ] at 248 nm (Supplementary Fig. SF4) as a function of temperature reflect only the equilibrium between the trans-tapered dendron and its aggregate, while the UV analysis demonstrates the progression of the conformational order of the dendron. For the aggregate in cyclohexane (1.6×10^{-4} M), a transition temperature T_m of 22 °C is calculated from UV, CD and NMR plots as a function of temperature. For clarity, the NMR data in Fig. 2a are reported at a higher concentration (2.0×10^{-3} M) and show, as expected, a higher T_m (32 °C).

Differential scanning calorimetry (DSC) (Fig. 3a), small-angle powder X-ray diffraction (XRD) (Fig. 3b) and wide-angle oriented fibre XRD (Fig. 3c) show that the supramolecular structures assembled in bulk from (4-3,4-3,5)12G2-CH_2-(L-Tyr-L-Ala) and (4-3,4-3,5)12G2-CH_2-(D-Tyr-D-Ala) exhibit identical transition temperatures and structure (Fig. 3a–c and Supplementary Table ST2). The CD spectra, tested for the absence of linear dichroism, and UV spectra of these dendrons recorded from cyclohexane solution or as thin films on quartz (Supplementary Fig. SF5) are identical except that L-L and D-D dendritic dipeptides show mirror-image Cotton effects (Fig. 2c, d). The similarity of the UV and CD spectra obtained from solution and in bulk indicates the same supramolecular structure in both states. The DL-DL, D-L and L-D dendritic dipeptides exhibit similar structures as the L-L and D-D (Fig. 3a–c) except that DL-DL, D-L and L-D dendritic dipeptides have slightly lower transition temperatures. Their helical sense is determined by the stereochemistry of Tyr. Thin-film CD spectra show this helical columnar structure in both ordered glassy and liquid crystalline states (Supplementary Fig. SF5). Although the DL-DL derived supramolecular structure is racemic, its fibre XRD demonstrates columns with short-range helical order (Fig. 3c). The presence of helicity in the columns of the racemic DL-DL dendritic

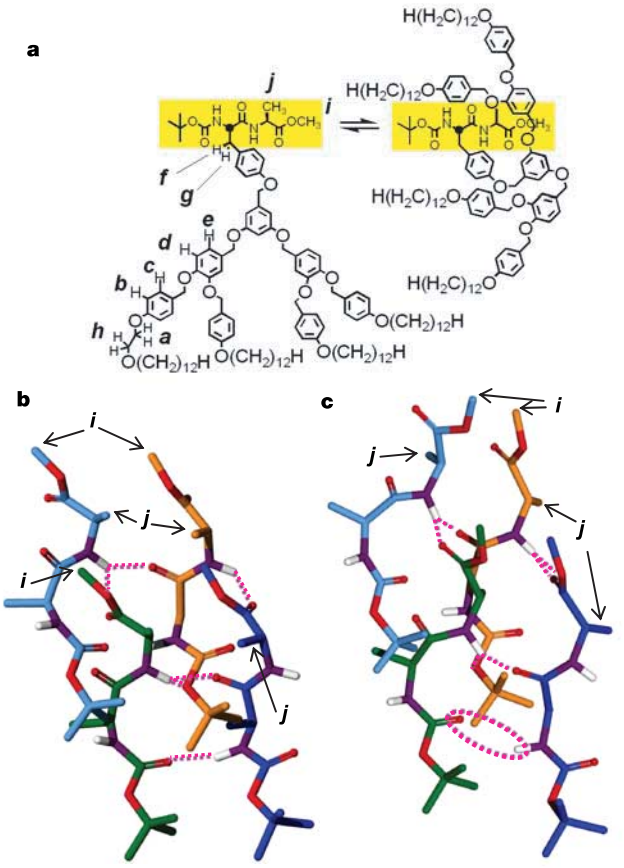

Figure 1 Structure, conformation and hydrogen-bonding of (4-3,4-3,5)12G2-CH_2-Boc-L-Tyr-L-Ala-OMe and (4-3,4-3,5)12G2-CH_2-Boc-L-Tyr-D-Ala-OMe during self-assembly. **a**, Trans-tapered low-temperature (left), and globular high-temperature (right), conformers of the L-L stereoisomer. The letters (*a, b,…j*), some of them also indicated in **b** and **c**, indicate protons with ^{1}H-NMR chemical shifts marked in Fig. 2a. Yellow indicates the region of the dendritic dipeptide where functional groups capable of taking part in hydrogen-bonding are accessible (left), and the corresponding region that sterically prevents the same type of hydrogen-bonding in the globular structure (right). **b**, Hydrogen-bonding interactions of the L-L dipeptide forming the pore according to the model from Fig. 4e. **c**, Hydrogen-bonding interactions of the L-D dipeptide. In **b** and **c**, four dipeptides from two layers are illustrated (top layer has one peptide with carbons shown light blue and one with carbons shown gold, bottom layer has one peptide with carbons shown green and one with carbons shown dark blue; oxygen, red; hydrogen, white; nitrogen, purple; phenyl of Tyr and hydrogens not shown except in hydrogen-bonding N-H). The L-D dipeptide does not exhibit (dotted oval) the bottom hydrogen-bonding of the L-L dipeptide. This explains the lower transition temperature of the L-D dendritic dipeptide assembly (Fig. 3a). Hydrogen-bonding distances are in Supplementary Fig. SF14.

©2004 Nature Publishing Group

dipeptide suggests that helix conformation is induced by the achiral dendrons, with the chiral peptide attached to the dendron only selecting the twist sense of the helix. This assembly behaviour relates to other examples of stereocentres determining the twist sense of racemic helical structures[20,21], and contrasts with systems where a stereocentre induces helicity in an achiral non-helical supramolecular structure[22,23].

Transmission electron microscopy (TEM) images and electron diffraction (ED) patterns (Fig. 3e) of the homeotropically aligned, and scanning force microscopy (SFM) images of the planar-aligned, two-dimensional hexagonal columnar lattice (Fig. 3f) confirm and complement the XRD analysis. Moreover, TEM images and their Fourier reconstructions show columns with low electron density both in the core and in their aliphatic periphery (Fig. 3e). These images contrast with previously observed TEM for closed-core columns with a high electron density in their core[17]. The low electron density in the core is associated with the hollow structure of the cylinder, and explains the anomalously enhanced intensities of the higher-order diffraction peaks (11), (20) and (21) observed in XRD (Fig. 3b) and ED (Fig. 3e). Absolute electron density profiles were computed from the XRD data (Supplementary Figs SF10 and SF11) assuming an intramolecular phase segregated column[14,24]. The phases of the (10), (11) and (20) reflections were established from the Fourier analysis of the TEM images (Supplementary Figs SF7 and SF8), and those of higher order reflections (21) and (30) were phase combinations that resulted in nearly constant electron density for the aromatic and aliphatic regions satisfying the intramolecular segregated model[17,24]. The converted electron density profiles (Supplementary Figs SF10 and SF11) of the assembly exhibit significantly lower electron density in the core than the average aliphatic density (approximately 0.30 electrons $Å^{-3}$ for a mass density of 0.86 g cm^{-3}) in the periphery and demonstrate hollow columns (Fig. 3d). Form-factor calculations were performed for a column model with three levels of electron density (hollow core, high density peptide-aromatic region, low density aliphatic periphery) distribution. These calculations, in combination with experimental densities, electron density profiles and molecular modelling experiments, were performed for the entire series of supramolecular structures generated from L-L dendritic dipeptides with $n = 6$, 8, 10, 12, 14 and 16 to determine their pore diameters (D_{pore}) and structure. The external diameters (D_{ext}) were calculated from the peak positions in the XRD[15,18] (Fig. 3b). Values of D_{pore} were obtained from the least-squares fit of the diffraction amplitudes calculated from the three level electron density model to the measured XRD amplitudes. The dendritic dipeptides with $n = 12$ and D-D, D-L, L-D and DL-DL stereochemistry have D_{pore} values of 13.6, 12.8, 13.7 and 12.8 Å.

The side view of the supramolecule generated from (4-3,4-3,5)12G2-CH_2-(L-Tyr-L-Ala), its top view (only methyl groups are shown as the alkyl groups of the dendron), the top view of a single layer of the pore, and the cross-section of the pore without the dendron, are shown in Fig. 4a–d. A right-handed column is self-assembled from the L-L dendritic dipeptide and a left-handed one from the D-D stereoisomer. The pore interior is hydrophobic, containing the methyl group of Ala (white) and one methyl group of the Boc (blue) on the pore surface. The hydrophilic part of the dipeptide is segregated between the hydrophobic dendron and the hydrophobic pore. Hydrophobic channels are important, because they facilitate the transport of ions[2] and water[3,25] with both high rate and selectivity. The conformation of the dendritic dipeptide and the hydrogen-bonding interactions that generate the supramolecular assembly and the inner part of the pore are illustrated in Fig. 1b, c and Supplementary Figs SF13 and SF14. The dipeptide forms an interdigitated and hydrogen-bonded β-helix[26] in response to the self-assembly of its dendritic fragment. The structure of the pore resembles a β-barrel[7,13]. The classic antiparallel dipeptide model[13] was eliminated first, as it does not form a column. Eight additional structures (four non-helical and four helical) of pore assembly were considered (Supplementary Fig. SF12) before selecting the model shown in Fig. 4e, which is stabilized via a hydrogen-bonding

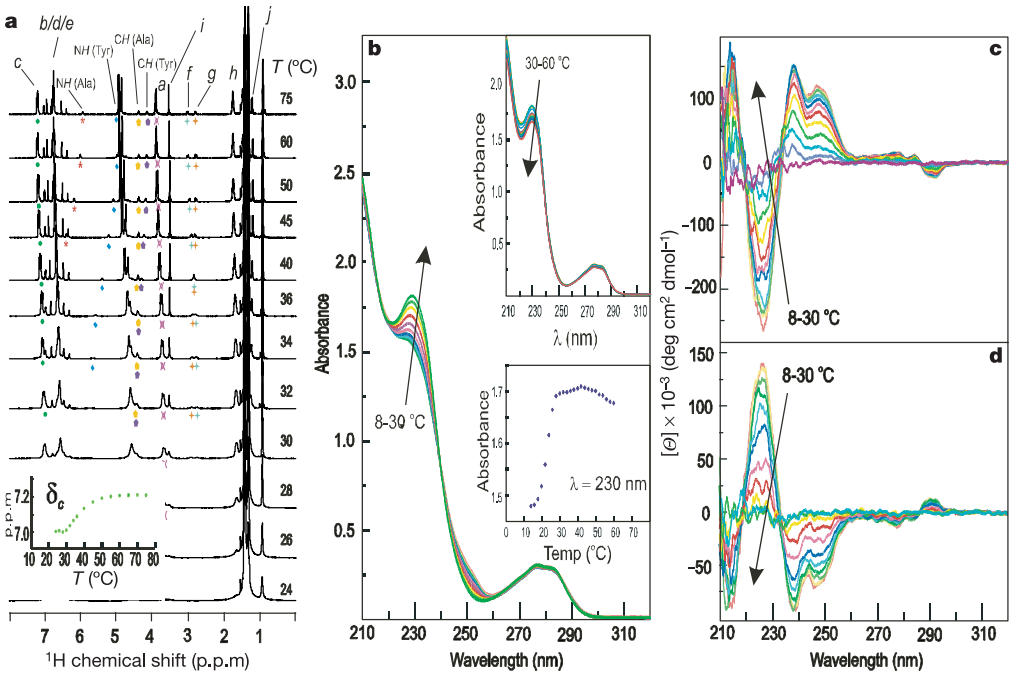

Figure 2 Spectroscopic analysis of dendritic dipeptide self-assembly in solvophobic solution. **a**, ^{1}H-NMR (500 MHz) spectra of (4-3,4-3,5)12G2-CH_2-Boc-L-Tyr-L-Ala-OMe in C_6D_{12} (2.0×10^{-3} M). Inset shows the plot of chemical shift, δ_c, as a function of temperature. Proton assignments are shown in Fig. 1. **b**, UV spectra of (4-3,4-3,5)12G2-CH_2-Boc-L-Tyr-L-Ala-OMe in cyclohexane (1.6×10^{-4} M) exhibiting an isosbestic point at 240 nm. Insets are spectra at higher temperature and a plot of A_{230} as a function of temperature. **c**, CD spectra of (4-3,4-3,5)12G2-CH_2-Boc-L-Tyr-L-Ala-OMe in cyclohexane (1.6×10^{-4} M). **d**, CD spectra of (4-3,4-3,5)12G2-CH_2-Boc-D-Tyr-D-Ala-OMe in cyclohexane (1.6×10^{-4} M). In all parts, arrows indicate trends upon increasing temperature.

©2004 Nature Publishing Group

network (Fig. 1b, c). This model is unrelated to that of the single crystal structure of the dipeptide without dendron (Supplementary Fig. SF15).

Figures 1b, c, Fig. 4 and Supplementary Fig. SF14 suggest methods to redesign the pore architecture by using the retro-structural analysis of its XRD generated structure[15,18]. For example, the replacement of Boc from (4-3,4-3,5)12G2-CH_2-(L-Tyr-L-Ala) with Moc reduced the pore diameter from 12.8 Å to 10.2 Å. The conformation of the phenyl from Tyr is anti with respect to its Boc group, and is tilted in the opposite direction (Supplementary Fig. SF13a). Therefore, attaching the dendron to Tyr via an ester rather than benzyl ether was expected to restrict its dynamics; this has been demonstrated by the structure of (4-3,4-3,5)12G2-CO_2-(L-Tyr-L-Ala), which, despite D_{pore} = 12.4 Å, requires longer annealing to achieve structural order as measured by XRD. The replacement of L-Ala from (4-3,4-3,5-)12G2-CH_2-(L-Tyr-L-Ala) with other non-polar or polar amino acids such as Gly, L-Val, L-Phen and L-Ser, of L-Tyr with L-Cys, of (L-Tyr-L-Ala) with (L-Ala-L-Tyr), and of (4-3,4-3,5)12G2- with other dendrons produced building blocks that self-assemble into related porous columns (Supplementary Tables ST6 and ST8). The smaller D_{pore} of (4-3,4-3,5)12G2-CH_2-[Boc-L-Cys-L-Ala-OMe] (10.0 Å versus 13 Å for the case of the same dendritic dipeptide with Boc-L-Tyr-L-Ala-OMe dipeptide) suggests that the phenyl group from Tyr plays an important role in the self-assembly of porous columns. Therefore, a library of self-assembling dendrons containing additional phenyl and biphenyl groups in their apex and/or branches was designed to produce 20 non-peptidic porous columns with D_{pore} ranging from 2 to 24 Å (Supplementary Tables ST9 to ST13). These structures, together with those generated from the 19 dendritic dipeptides (Supplementary Tables ST5 to ST8), demonstrate the simplicity and versatility of this approach to the fabrication of both non-biological pores and tubular liquid crystals[10,11].

Successful self-assembly of the dendritic dipeptides in cyclohexane suggests that they may also assemble in phospholipid membranes, and suitable decoration of their alkyl groups might mediate their assembly in or on the surface of microbial cell membranes[5]. As first step in this direction, the porous structure of (4-3,4-3,5)12G2-

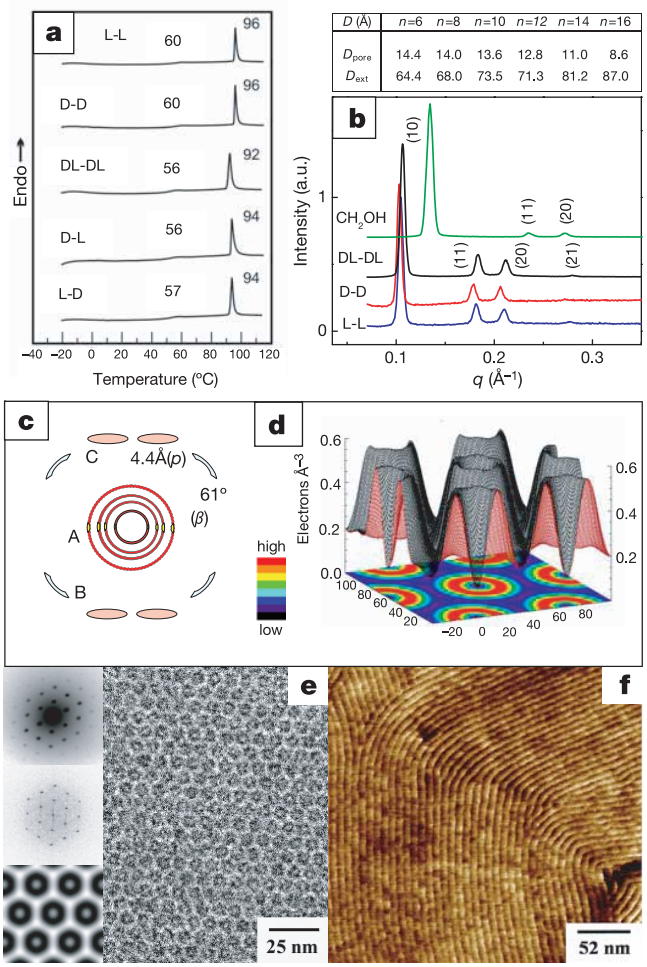

D (Å)	n=6	n=8	n=10	n=12	n=14	n=16
D_{pore}	14.4	14.0	13.6	12.8	11.0	8.6
D_{ext}	64.4	68.0	73.5	71.3	81.2	87.0

Figure 3 Structural analysis of dedritic dipeptide pore in bulk. **a**, DSC showing the glassy and isotropization temperatures of L-L, D-D, DL-DL, D-L and L-D stereoisomers of (4-3,4-3,5)12G2-CH_2-Boc-Tyr-Ala-OMe. **b**, Powder XRD of L-L, D-D and DL-DL stereoisomers of (4-3,4-3,5)12G2-CH_2-Boc-Tyr-Ala-OMe and of (4-3,4-3,5)12G2-CH_2OH. Also shown (top table) are D_{ext} and D_{pore} (Å) of (4-3,4-3,5)nG2-CH_2-Boc-L-Tyr-L-Ala-OMe with n = 6 to 16. **c**, Wide and small-angle fibre XRD pattern. A, column to column distance, long-range order; B, molecular tilt (β); C, short-range helical correlation along column axis, short-range pitch (p). **d**, Electron density maps of (4-3,4-3,5)12G2-CH_2-Boc-L-Tyr-L-Ala-OMe columns. Profile shows variation of electron density in a plane perpendicular to columns. Coloured contour maps show change in electron density in the same plane (x and y axes of the plane are in Angströms). **e**, TEM of (4-3,4-3,5)12G2-CH_2-Boc-L-Tyr-L-Ala-OMe along the column axis. Insets from top are: electron diffraction pattern, Fourier transform power spectrum, and image reconstructed from the (10), (11) and (20) Fourier components with phases: +, −, −. **f**, SFM of columns parallel to pyrolytic graphite substrate. Dislocations and disclinations of the focal conic like texture are observed.

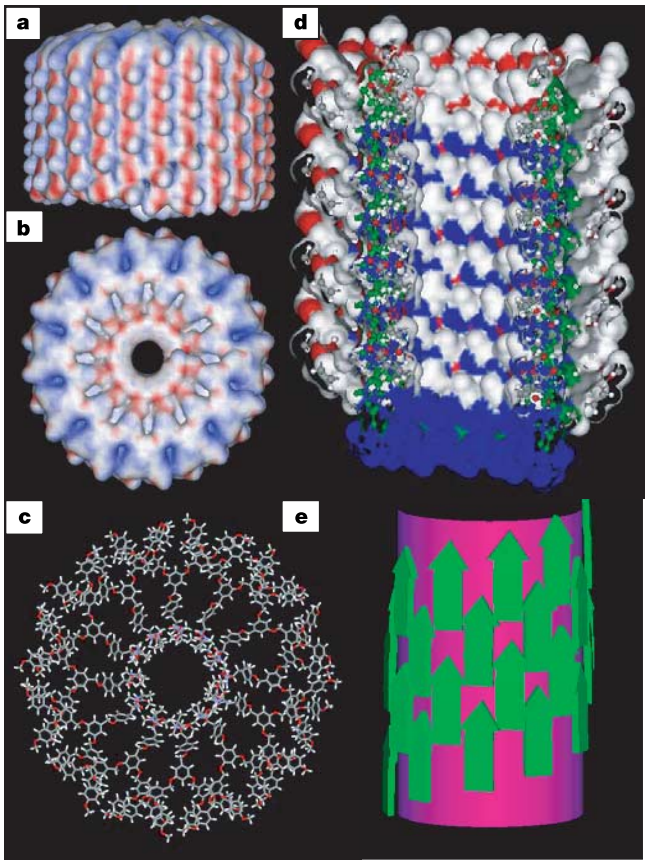

Figure 4 Molecular models of the helical porous columns self-assembled from (4-3,4-3,5)12G2-CH_2-Boc-L-Tyr-L-Ala-OMe (for simplicity n = 12 was replaced with n = 1). **a**, Side view of the right-handed column. **b**, Top view of **a**. **c**, Top view of a single porous column layer. **d**, Cross-section through the hydrophobic pore (without dendrons) showing its β-barrel structure (CH_3 of Ala is white, CH_3 of Boc are blue, O is red, C-N of dipeptide are green, aromatic groups are grey) assembled from the β-helical dipeptides. **e**, Schematic model for the self-assembly of the dipeptidic β-barrel pore. The green arrows indicate the dipeptides.

©2004 Nature Publishing Group

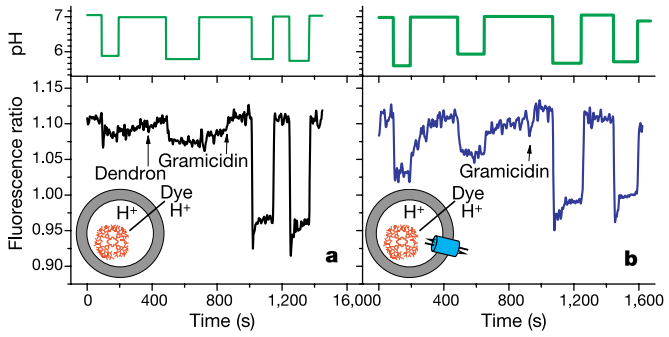

Figure 5 Proton transport through (4-3,4-3,5)12G2-CH_2-(Boc-L-Tyr-L-Ala-OMe) pores reconstituted in phospholipid liposomes (pH-jump experiments). **a**, Liposomes containing only the membrane-impermeable pH indicator[28] inside. **b**, Liposomes containing the pH indicator inside and the dendritic dipeptide pores. In both cases, arrows indicate the addition of the dendritic dipeptide or gramicidin as DMSO/THF solutions. pH jumps at 20 °C outside the liposome (induced by adding aliquots, about 10 μl, of HCl or KOH) were recorded by pH microelectrodes (upper graphs). pH jumps inside liposomes were assessed by fluorescence (I_{647}/I_{670}) (lower graphs). The signal of the total amount of captured pH dye was estimated by adding an excess of gramicidine. Liposomes were prepared by sonicating a 1/14 mass ratio of dendritic dipeptide in the presence of L-α-phosphatidylcholine (P5638 from Sigma) and a fluorescent membrane-impermeable pH indicator (G4 polyglutamic porphyrin-dendrimer)[28] in a phosphate buffer (10 mM K_2HPO_4, 50 mM KCl, pH = 7.0). The control experiment (**a**) has no dendron. Liposomes were purified from untrapped indicator by gel filtration on Sephadex (G200) and on anion exchange resin QAE Sepharose A50 and placed in a fluorimetric cell equipped with a stirrer. As expected from its hydrophobicity (un-optimized experiment **a**), the dendritic dipeptide was not delivered very effectively to liposomes by simply adding its solution in DMSO/THF: the addition increases permeability only slightly. In contrast, liposomes made of a lipid dendritic dipeptide mixture[27] (14/1 mass ratio lipid to dendron equivalent to an average of one to two pores per vesicle; Supplementary Section S10) yields permeable vesicles significantly more responsive to pH changes (**b**). Addition of gramicidin increases the magnitude of the jumps, suggesting that a small fraction of vesicles did not contain dendritic channels. Addition of 10 μl of DMSO alone does not affect permeability.

CH_2-[Boc-L-Tyr-L-Ala-OMe] was reconstituted[27] in the thermotropic bilayer lamellar phase and in liposomes produced from phospholipids (Supplementary Section S9). By monitoring the emission intensity of a pH-sensitive fluorescent dye[28] captured inside the liposomes, proton translocation mediated by dendritic pores and gramicidin channels can be evaluated (Fig. 5 and Supplementary Fig. SF19)[28,29]. Proton permeability of liposomes containing an average of one to two reconstituted dendritic pores (14/1 mass ratio phospholipid to dendritic dipeptide) was comparable in efficiency to those containing gramicidin channels. These results illustrate that supramolecular dendrimer chemistry[30] allows the controlled design of a range of periodic non-biological porous structures forming in solution and as films. □

Received 11 February; accepted 16 June 2004; doi:10.1038/nature02770.

1. Klug, A. From macromolecules to biological assemblies. *Angew. Chem. Int. Edn Engl.* **22,** 565–582 (1983).
2. Doyle, D. A. *et al.* The structure of the potassium channel: molecular basis of K^+ conduction and selectivity. *Science* **280,** 69–77 (1998).
3. Murata, K. *et al.* Structural determinants of water permeation through aquaporin-1. *Nature* **407,** 599–605 (2000).
4. van den Berg, B. *et al.* X-ray structure of a protein conducting channel. *Nature* **427,** 36–44 (2004).
5. Fernandez-Lopez, S. *et al.* Antibacterial agents based on the cyclic D,L-α-peptide architecture. *Nature* **412,** 452–455 (2001).
6. Ishii, D. *et al.* Chaperonin-mediated stabilization and ATP-triggered release of semiconductor nanoparticles. *Nature* **423,** 628–632 (2003).
7. Bayley, H. & Cremer, P. S. Stochastic sensors inspired by biology. *Nature* **413,** 226–230 (2001).
8. Ghadiri, M. R., Granja, J. R., Millligan, R. A., McRee, D. E. & Khazanovich, N. Self-assembling organic nanotubes based on a cyclic peptide architecture. *Nature* **366,** 324–327 (1993).
9. Schmitt, J.-L., Stadler, A.-M., Kyritsakas, N. & Lehn, J.-M. Helicity encoded molecular strands: efficient access by the hydrazone route and structural features. *Helv. Chim. Acta* **86,** 1598–1624 (2003).
10. Lehn, J.-M. *Supramolecular Chemistry. Concepts and Perspectives* 118 (VCH, Weinheim, 1995).
11. Bong, D. T., Clark, T. D., Granja, J. R. & Ghadiri, M. R. Self-assembling organic nanotubes. *Angew. Chem. Int. Edn Engl.* **40,** 989–1011 (2001).
12. Hill, D. J., Mio, M. J., Prince, R. B., Hughes, T. S. & Moore, J. S. A field guide to foldamers. *Chem. Rev.* **101,** 3893–4011 (2001).
13. Sakai, N. & Matile, S. Synthetic multifunctional pores: lessons from rigid-rod β-barrels. *Chem. Commun.*, 2514–2523 (2003).
14. Percec, V. *et al.* Controlling polymer shape through the self-assembly of dendritic side-groups. *Nature* **391,** 161–164 (1998).
15. Percec, V. *et al.* Self-organization of supramolecular helical dendrimers into complex electronic materials. *Nature* **419,** 384–387 (2002).
16. Percec, V., Cho, W.-D., Ungar, G. & Yeardley, D. J. P. Synthesis and NaOTf mediated self-assembly of monodendritic crown-ethers. *Chem. Eur. J.* **8,** 2011–2025 (2002).
17. Hudson, S. D. *et al.* Direct visualization of individual cylindrical and spherical dendrimers. *Science* **278,** 449–452 (1997).
18. Percec, V., Cho, W.-D., Ungar, G. & Yeardley, D. J. P. Synthesis and structural analysis of two constitutional isomeric libraries of AB_2-based monodendrons and supramolecular dendrimers. *J. Am. Chem. Soc.* **123,** 1302–1315 (2001).
19. Nelson, J. C., Saven, J. G., Moore, J. S. & Wolynes, P. G. Solvophobically driven folding of nonbiological oligomers. *Science* **277,** 1793–1796 (1997).
20. Brunsveld, L., Zhang, H., Glasbeek, M., Vekemans, J. A. J. M. & Meijer, E. W. Hierarchical growth of chiral self-assembled structures in protic media. *J. Am. Chem. Soc.* **122,** 6175–6182 (2000).
21. Chan, H. S., Bromberg, S. & Dill, K. A. Models of cooperativity in protein folding. *Phil. Trans. R. Soc. Lond. B* **348,** 61–70 (1995).
22. Engelkamp, H., Middelbeek, S. & Nolte, R. J. M. Self-assembly of disk-shaped molecules to coiled-coil aggregates with tunable helicity. *Science* **284,** 785–788 (2001).
23. Hirschberg, J. H. K. K. *et al.* Helical self-assembled polymers from cooperative stacking of hydrogen-bonded pairs. *Nature* **407,** 167–170 (2000).
24. Balagurusamy, V. S. K., Ungar, G., Percec, V. & Johansson, G. Rational design of the first spherical supramolecular dendrimers self-organized in a novel thermotropic cubic liquid-crystalline phase and the determination of their shape by X-ray analysis. *J. Am. Chem. Soc.* **119,** 1539–1555 (1997).
25. Hummer, G., Rasaiah, J. C. & Noworita, J. P. Water conduction through the hydrophobic channel of a carbon nanotube. *Nature* **414,** 188–190 (2001).
26. Cornelissen, J. J. L. M. *et al.* β-Helical polymers from isocyanopeptides. *Science* **293,** 676–680 (2001).
27. Rigaud, J.-L., Pitard, B. & Levy, D. Reconstitution of membrane proteins into liposomes: application to energy-transducing membrane proteins. *Biochim. Biophys. Acta* **1231,** 223–246 (1995).
28. Finikova, O. *et al.* Porphyrin and tetrabenzoporphyrin dendrimers: tunable membrane-impermeable fluorescent pH nanosensors. *J. Am. Chem. Soc.* **125,** 4882–4893 (2003).
29. Ghadiri, M. R., Granja, J. R. & Buehler, L. K. Artificial transmembrane ion channels from self-assembling peptide nanotubes. *Nature* **369,** 301–304 (1994).
30. Emrick, T. & Fréchet, J. M. J. Self-assembly of dendritic structures. *Curr. Opin. Colloid Interface Sci* **4,** 15–23 (1999).

Supplementary Information accompanies the paper on **www.nature.com/nature**.

Acknowledgements Financial support by the National Science Foundation, the Office of Naval Research and the P. Roy Vagelos Chair at the University of Pennsylvania is acknowledged. J.S. thanks the Isabel and Alfred Bader Foundation for a graduate fellowship, and U.E. acknowledges a Hans Werthén scholarship for postdoctoral studies. We also thank S.Z.D. Cheng for density measurements, and G. Ungar for reading the draft manuscript and for suggestions.

Competing interests statement The authors declare that they have no competing financial interests.

Correspondence and requests for materials should be addressed to V.P. (percec@sas.upenn.edu).

Quantification of modelling uncertainties in a large ensemble of climate change simulations

James M. Murphy[1], David M. H. Sexton[1], David N. Barnett[1], Gareth S. Jones[1], Mark J. Webb[1], Matthew Collins[1] & David A. Stainforth[2]

[1]*Hadley Centre for Climate Prediction and Research, Met Office, FitzRoy Road, Exeter EX1 3PB, UK*
[2]*Department of Physics, University of Oxford, Parks Road, Oxford OX1 3PU, UK*

Comprehensive global climate models[1] are the only tools that account for the complex set of processes which will determine future climate change at both a global and regional level. Planners are typically faced with a wide range of predicted changes from different models of unknown relative quality[2,3], owing to large but unquantified uncertainties in the modelling

©2004 Nature Publishing Group